Lawrence Berkeley National Laboratory
Recent Work

Title

Thermodynamic analysis of a novel fossil-fuel–free energy storage system with a trans-critical carbon dioxide cycle and heat pump

Permalink
https://escholarship.org/uc/item/3hh9c0n0

Journal
International Journal of Energy Research, 44(10)

ISSN
0363-907X

Authors
Hao, Y
He, Q
Liu, W
et al.

Publication Date
2020-08-01

DOI
10.1002/er.5130

Peer reviewed

eScholarship.org Powered by the California Digital Library
University of California

Thermodynamic Analysis of a Novel Fossil-Fuel-Free Energy Storage System with a Trans-Critical Carbon Dioxide Cycle and Heat Pump

Yinping Hao[a,b], Qing He[a,*], Wenyi, Liu[a], Lehua Pan[b], Curtis M. Oldenburg[b]

[a]School of Energy Power and Mechanical Engineering, North China Electric Power University, No.2 Beinong Road, Changping, Beijing 102206, China

[b]Energy Geosciences Division, 74-316C, Lawrence Berkeley National Laboratory, Berkeley, CA 94720, USA

Abstract: This paper presents and analyzes a novel fossil-fuel-free trans-critical energy storage system that uses CO_2 as the working fluid in a closed loop shuttled between two saline aquifers or caverns at different depths, one a low-pressure reservoir, and the other a high-pressure reservoir. Thermal energy storage and a heat pump are adopted to eliminate the need for external natural gas for heating the CO_2 entering the energy recovery turbines. We carefully analyze the energy storage and recovery processes to reveal the actual efficiency of the system. We also highlight thermodynamic and sensitivity analyses of the performance of this fossil-fuel-free trans-critical energy storage system based on a steady-state mathematical method. It is found that the fossil-fuel-free trans-critical CO_2 energy storage system has good comprehensive thermodynamic performance. The exergy efficiency, round-trip efficiency, and energy storage efficiency are 67.89%, 66% and 58.41%, and the energy generated of per unit storage volume is 2.12 kW·h/m^3, and the main contribution to exergy destruction is the turbine re-heater, from which we can quantify how performance can be improved. Moreover, with a relatively higher energy storage and recovery pressure and lower pressure in the low-pressure reservoir, this novel system shows promising performance.

Keywords: fossil-fuel-free, compressed trans-critical CO_2, subsurface energy storage, heat pump, thermodynamic analysis, sensitivity analysis

Note: This is the manuscript form of a published paper and may differ slightly from the final published paper. Please read and cite the final published paper:

Hao, Y., He, Q., Liu, W., Pan, L. and Oldenburg, C.M., Thermodynamic analysis of a novel fossil-fuel–free energy storage system with a trans-critical carbon dioxide cycle and heat pump. *International Journal of Energy Research*.

*Corresponding author:
E-mail address: hqng@163.com (Qing He).

1. Introduction

Increasing energy demand and rising concern about greenhouse gas emissions from fossil-fuel power generation have led to worldwide interest in renewable energy sources [1]. Rapid development and worldwide utilization of renewable energy sources bring not only diversification of the global energy industry, but also challenges in integrating renewable energy such as wind and solar energy into the electricity grid due to intermittency and instability over a wide range of time scales from short (minute) to long (seasonal) [2-5]. In order to optimize integration of wind and solar power into the electricity grid, practical large-scale (bulk) energy storage systems (ESS) are urgently needed. The technologies currently are available to provide bulk energy storage include pumped hydro storage (PHS) and compressed air energy storage (CAES) [6-8]. The development of batteries for bulk energy storage is ongoing, but there are only a few utility-scale stationary battery storage projects in place for long-term (daily) storage and these systems are expensive and provide only a small fraction of energy stored by pumped hydro storage [9,10].

It is well known that the only two current operating conventional CAES plants rely on natural gas for energy recovery resulting in greenhouse gas emissions. The fact that renewable energy stored by CAES may result in greenhouse gas emissions upon energy recovery has motivated thinking about novel CAES systems, some of which can avoid the need for natural gas. Among the many novel CAES systems that have been proposed are the super-critical CAES (SC-CAES) [11], porous media CAES (PM-CAES) [12], and small scale CAES [13]. In addition, several new approaches to adiabatic CAES have recently been introduced. For example, advanced adiabatic CAES (AA-CAES) [14-16] and high-temperature adiabatic CAES [17] have been analyzed and show potential to solve the economic and environmental challenges related to the use of fossil fuel combustion during energy recovery. Thermodynamic analyses have become standard for these systems for design and efficiency analyses [18-20]. Several of new CAES systems [21, 22] have been proposed to improve thermal efficiency of CAES, and liquefied air energy storage (LAES) [23, 24] has been studied to improve energy storage density.

Recently, growing interest has been focused on the use of carbon dioxide (CO_2) in compressed gas storage because of its unique properties and characteristics. Utilizing CO_2 instead of air in compressed gas energy storage will not only improve the system performance but also offer a possibility for utilization of CO_2 with corresponding reductions in carbon emission [25]. Wu et al. [26] proposed a novel trans-critical compressed CO_2 energy storage system that showed good performance, energy storage density, and high efficiency. Liu et al. [27] proposed a system that combined compressed gas energy storage in deep subsurface reservoirs (porous media or caverns) and utilization of CO_2 which gets much higher energy density and good energy storage efficiency. Buscheck et al. [28] were investigating ways to exploit deep reservoirs for both their ability to store CO_2 beneficially in both the geologic carbon sequestration context and for energy storage, including exploitation of natural geothermal heating of the CO_2. Ahmadi et al [29-32] explored a few of novel CO_2 power cycles and thermodynamic optimizations on these systems have been performed. Mehmet et al. [33] posed novel electro-thermal energy storage with trans-critical CO_2 cycles, aiming to make improvement on the CO_2 machines and the system performance. An optimization on thermodynamic performance of the turbine turbomachinery in an energy storage system with CO_2 as working fluid has been performed [34]. Based on CO_2 in a Brayton cycle, a compressed CO_2 energy storage cycle has been proposed and thermodynamic optimization showed much better thermal performance compared with other CAES systems [35].

Based on the above research, the development of compressed gas energy storage utilizing CO_2 as working fluid has become a focus of research and development. In this paper, we present and analyze a novel closed-loop energy storage system that uses CO_2 as the working fluid that is cycled between high-pressure and low-pressure reservoirs. The innovation highlight in this system is that we analyze the use of a heat pump instead of fossil fuel to recover and reheat stored heat of compression during the energy recovery process. We present mathematical thermodynamic models of the proposed compressed trans-critical CO_2 energy storage system, and carry out parametric analyses to examine the effects on system performance of key thermodynamic parameters.

2. System description

We propose a closed-loop energy storage system that takes advantage of the large volumes and remote subsurface locations of saline aquifers or large storage caverns for hosting two CO_2 storage reservoirs. One reservoir is low-pressure, and the other is high-pressure, which serve to store, respectively, CO_2 entering the electricity-producing turbines, and CO_2 following compression in the storage cycle. In this novel energy storage system, the CO_2 transitions from supercritical state to gaseous state in the turbines, which is denoted as a trans-critical compressed CO_2 energy storage (TC-CCES). The schematic of this novel TC-CCES is depicted in Fig. 1, and its T-S graph is illustrated in Fig. 2. The schematic of the heat pump sub-system of the TC-CCES system is shown in Fig. 3.

2.1 Energy storage process

As shown in Fig. 1, the green background represents the energy storage process (compression phase), and the orange background represents the energy recovery process (generation phase). The overlapping region in the middle includes the heat storage unit, cold storage unit, and low- and high-pressure reservoirs (LR and HR), all of which are involved in both energy storage and energy recovery process.

The working principle of the storage process is as follows:

(a) 14-1: The working fluid (trans-critical CO_2) stored in LR is cooled through a pre-cooler (PC) and injected into the compressor, with the heat of compression (19-20) stored in the heat storage unit.

(b) 1-2, 3-4, 5-6: During hours when excess renewable electricity is available, the CO_2 is pressurized in the compressor to temperatures and pressures above the critical point (304.15K, 7.4 MPa).

(c) 2-3, 4-5: The compressed CO_2 heats up in the process, and is then cooled by the inter-cooler heat exchangers (IC1 and IC2), and the heat generated during the compression process (15-16, 17-18) is stored in the heat storage unit.

(d) 6-7: The compressed CO_2 with high temperature and pressure then is directly injected into HR for storage.

2.2 Energy recovery process

The working principle of the recovery process is as follows:

(a) 7-8: CO_2 at high temperature and high pressure, potentially with additional geothermal heat absorbed from the deep reservoir, is adjusted to a fixed pressure through the high-pressure valve, and is fed into the energy recovery turbine.

(b) 8-9, 10-11, 12-13: The high-pressure CO_2 powers the turbines resulting in strong cooling of the CO_2, which is then fed into LR.

(c) 9-10, 11-12: The CO_2 exhausted from the turbines in front (8-9 or 10-11) is too cold to feed the next turbines (10-11 or 12-13). This exhausted CO_2 is reheated in TR1 or TR2 to prevent liquid CO_2 from forming and to provide enough volume throughput to drive each turbine. This reheating is accomplished using the heat provided by the hot water from the heat storage unit added by the heat pump system.

(d) 22-23: The temperature of the hot water stored in the heat storage unit (21-22) after absorbing the CO_2 compression heat is not high enough to reheat the exhausted CO_2 in the generation turbine train. Therefore, the hot water withdrawn from the heat storage unit is further heated by means of the heat pump (27-23) to raise its temperature to a required level. This heat pump is the key new feature of the system included to obviate the need for natural gas in the energy recovery process.

2.3 Heat pump system

The term high-temperature heat pump (HTHP) is frequently used in connection with industrial heat pumps, mainly for waste heat recovery in process heat supply [36]. In the compression system proposed here, the temperature of the heat storage unit would not be sufficient to maintain CO_2 pressure after exiting from Turbine 1 to drive Turbine 2, and similarly for exiting from Turbine 2 to drive Turbine 3 to generate electricity. What is needed is a way to transfer the waste heat stored in the heat storage unit which is at approximately 383K into the exhaust streams of the turbines which are at a temperature of approximately 363K. Due to the relatively high inlet temperature (approximately 423K) of Turbine 2, a heat pump is needed to make full use of the stored waste heat.

In selecting a working fluid for the heat pump, we prioritized efficient and steady performance along with low environmental impact factor and high safety. We found that R245fa is a low-pressure, high-temperature, and environmentally safe fluid with a high enough critical temperature (427K) for use as the heat pump working fluid [36, 37]. We evaluated the thermodynamic properties of R245fa using PEFPROP [38]. The physical properties of R245fa are given in Table 1. The schematic of the heat pump is illustrated in Fig. 3. The working principle of the heat pump can be described as:

(a) 29-30: R245fa is compressed during a non-isentropic process.

(b) 30-31: Gaseous high-pressure R245fa is cooled by hot water from the heat storage unit (22) resulting in condensation that provides latent heat to the water exiting (23) to the turbine exhaust heating loop at a specified temperature (433.15K).

(c) 31-32: Liquid R245fa expands through the expansion valve in a non-isentropic process.

(d) 32-29: Liquid R245fa is heated through the evaporator by water from the turbine exhaust cooling loop (27) causing R245fa to vaporize and causing cooling of the water that exits to the 'cold' water storage tank.

3. Theoretical model

For simplicity, we make the following assumptions about the proposed TC-CCES:

(a) The TC-CCES system uses the thermodynamic model based on the thermodynamic law and operates at steady-state conditions, and we ignore pressure drops and heat losses in the pipes, heat exchangers, heat storage tank, and heat pump. The water stored in the cold storage unit will be cooled down to room temperature (298.15K) before it is used to cool the CO_2 from LS being fed to the compressor train.

(b) Equal CO_2 mass flow rates are assumed during the energy storage process (withdrawing CO_2 from the LR and injecting CO_2 at high-pressure into the HR) and the energy recovery process (withdrawing high-pressure CO_2 from the HR and injecting low-pressure CO_2 into the LR).

(c) The system is closed (there are no losses of CO_2 within the storage reservoirs or in the above-ground facility) and the stored energy of compression is large enough that we can neglect kinetic and potential energy changes as CO_2 flows through the closed-loop system. In addition, the details of wellbore flow are ignored in the analysis and we assume constant wellhead P-T conditions during withdrawal and injection periods.

3.1 Compressor train

The compressors used for storing energy have isentropic efficiencies given by

$$\eta_c = \frac{h''_{i,s} - h'_i}{h''_i - h'_i} \tag{1}$$

where, h'_i is the enthalpy of inlet compressor; $h''_{i,s}$ is the isentropic enthalpy of outlet compressor; h''_i is the real entropy of outlet compressor; and i is the stage of compressor train, i = 1, 2, 3.

The power consumed by compression $W_{c,i}$ is

$$W_{c,i} = h''_i - h'_i \tag{2}$$

3.2 Turbine train

The turbines used for recovering energy have efficiencies and power needs analogous to those of the compressors. The isentropic efficiency of expansion in the turbine η_T is

$$\eta_T = \frac{h'_j - h''_{j,s}}{h'_j - h''_j} \tag{3}$$

where, h'_j is the enthalpy of inlet turbine; $h''_{j,s}$ is the isentropic enthalpy of the outlet turbine; h''_j is the real enthalpy of the outlet turbine; and j is the stage of the turbine train, j=1, 2, 3.

The power output during expansion by the turbine $W_{T,j}$ is

$$W_{T,j} = h'_j - h''_j \tag{4}$$

3.3 Storage model

For a saline aquifer storage reservoir, the groundwater in the aquifer has a pressure

P_{hs} given by

$$P_{hs} = \rho_w g Z \tag{5}$$

The LR is envisioned to be located at a shallower depth than the HR because the CO_2 well bottom pressure must exceed the reservoir pressure for injection to occur. Cavern pressures are more flexible, and there are no a priori restrictions on the depths of the low- and high-pressure reservoirs for caverns.

Similar to pressure, temperature increases with depth as given by the geothermal gradient, G, making T at any depth given by

$$T = T_s + GZ \tag{6}$$

where, T_s is the temperature at the ground surface.

To estimate saline aquifer reservoir volume, V_s is calculated from the following equations,

$$V_s = \frac{M_{co_2}}{(\rho'_{co_2} - \rho''_{co_2})} \tag{7}$$

3.4 Heat exchanger model

Both inter coolers and heaters of this system are applicable to the following model. The model for the heat-exchange processes involving CO_2 must be divided up into small steps to accommodate the large changes in CO_2 properties that occur as the temperature changes around the CO_2 critical point [39]. In the inter cooler between two compressors, the working fluid on the hot-stream side and cold-stream side are CO_2 and water, respectively. We suppose that the temperature difference ΔT on the hot-stream side is fixed and separated into N equal parts. Therefore, the heat transfer rate for the k-th part and mass flow rate of water can be illustrated below,

$$\dot{Q}_{he,k} = \dot{m}_{CO_2} C_{P,CO_2,k} \left(T_{CO_2,k} - T_{CO_2,k+1}\right) \tag{8}$$

$$\dot{Q}_{he,k} = \dot{m}_w C_{p,w,k} \left(T_{w,k+1} - T_{w,k}\right) \tag{9}$$

$$\dot{m}_w = \frac{\sum_k^N \dot{Q}_{he,k}}{(h_{w,out} - h_{w,in})} \tag{10}$$

3.5 Heat pump system

The high-temperature heat pump system is composed of a compressor, a condenser, an expansion valve, and an evaporator.

3.5.1 Compressor

Similar to the energy storage compressor, but with R245fa as working fluid instead of CO_2, the principal calculation is the same as that of energy storage compressor.

3.5.2 Condenser

In the heat pump condenser, the working fluids on both the hot-stream side and cold-stream side are R245fa and water, respectively. The mass flow rate of water is modeled by the equations

$$\dot{Q}_{he} = \dot{m}_{R245fa} C_{p,R245fa} \left(T'_{R245fa} - T''_{R245fa}\right) \tag{11}$$

$$\dot{Q}_{he} = \dot{m}_w C_{p,w} (T''_w - T'_w) \tag{12}$$

$$\dot{m}_w = \frac{\dot{Q}_{he}}{(h''_w - h'_w)} \tag{13}$$

3.5.3 Evaporator

In the evaporator of heat pump, R245fa is on the cold-stream side and water is on the hot-stream side. The principal calculation is the same as that of the condenser of the heat pump, except that the hot and cold streams are swapped.

3.5.4 Expansion valve

The expansion valve expands and depresses in the heat pump system and the entropies in the front and rear valves are equal, so the power is zero.

4. Performance criteria

To evaluate and compare the performance of the proposed TC-CCES system, we calculate the energy round-trip efficiency, energy storage efficiency, exergy efficiency, and energy generated per unit volume as quantities indicative of performance [40, 41].

4.1 Energy analysis

4.1.1 Round-trip efficiency

In general, for an energy cycle, the round-trip efficiency is often used to measure the performance of power unit that has an energy storage component. Round-trip efficiency is defined as the ratio of the electricity output during the recovery phase over the sum of the electricity consumed during the storage phase and the electricity (or equivalent energy) consumed during recovery phase [41], specifically,

$$\eta_{RT} = \frac{E_T}{E_C + \sum E_i} \tag{14}$$

where, E_T is the electricity output in the energy recovery process; E_C represents the total energy consumed during the energy storage process, and $\sum E_i$ is the electricity (or equivalent energy, e.g., natural gas converted into electricity in a conventional CAES power plant) consumed in the recovery process.

In the TC-CCES presented here, the latter term in Eq. (14) is the electricity used to power the heat pump.

4.1.2 Energy storage efficiency

While round-trip efficiency is a useful measure of the efficiency of a power plant with storage component, it is not a direct measurement of storage efficiency, i.e., how much stored energy can be recovered, because the large portion of electricity output may come from added natural gas during recovery in a conventional CAES system. As a result, it may be misleading to compare the efficiency of a CAES system against a battery-based electricity storage system using round-trip efficiency because the natural gas added during recovery in a conventional CAES system is really not a part of storage. To facilitate the comparison of storage efficiency across different type storage systems, we introduce a new performance criterion, named energy storage efficiency, which is defined as the ratio of the net energy that can be recovered from the system over the energy that consumed during storage:

$$\eta_{ES} = \frac{E_T - \sum E_i}{E_C} \tag{15}$$

where, $E_T - \sum E_i$ is the net energy recovered from storage process.

4.1.3 Energy generated per unit volume

The energy generated per unit volume of storage (EGV) for a TC-CCES system with two saline reservoirs is

$$\mathrm{EGV} = \frac{E_{GEN}}{V_s} = \frac{W_T \cdot t_{recovery}}{V_s} \tag{16}$$

4.2 Exergy analysis

Approaches for improving the performance of the system can be found by energy flow analysis. Therefore, we have carried out an exergy analysis to calculate exergy destruction in the TC-CCES system and its components.

The n^{th} component of the system can be described by its exergy balance equation [42, 43]

$$\dot{E}_{d,n} = \dot{E}_{F,n} - \dot{E}_{P,n} \tag{17}$$

where, $\dot{E}_{d,n}$, $\dot{E}_{F,n}$ and $\dot{E}_{P,n}$ are the exergy destruction rate, fuel exergy rate, and the product exergy rate, respectively.

We define exergy efficiency as

$$\eta_{EX} = \frac{E_P}{E_F} \tag{18}$$

The equations we use to calculate the component-by-component exergy destruction are listed in Table 2. Each component (*n*) of the system has an exergy destruction ratio defined as

$$X^*_{d,n} = \frac{\dot{E}_{d,n}}{\dot{E}_{F,n}} \tag{19}$$

5. Results and discussion

The properties of the system as summarized in Table 3 were used for the simulations and parametric analysis.

5.1 Thermodynamic analysis

Due to the use of an underground gas storage environment in the TC-CCES system, the temperature of CO_2 stored in HR may change in three different ways depending on the local geothermal gradient. (1) CO_2 could gain geothermal energy from the rock and become hotter; (2) heat stored in the CO_2 could be absorbed by rock in the HR region and cool; or (3) the CO_2 may neither gain nor lose heat and instead stay at approximately the same temperature. The thermodynamic analysis presented here assumes the first case because HR is likely to be deep whether it is an aquifer or a cavern. The analysis results of the TC-CCES system with heat pump are presented in Table 4, and the results of the power of compressors, turbines and heat pump are shown in Table 5. The results of the system efficiency and EGV are shown in Table 6. A summary of the results of performance criteria of the TC-CCES system and the results in [27] are shown in Table 7. The value of η_{RT} and η_{EX} of the TC-CCES system are 66.00% and 67.89%, respectively, which are better than the corresponding 63.35% and 53.02% in [27]. In particular, we find the value of η_{ES} is 58.41%, which is almost three times that in [27]. We also find that the energy generated per unit storage volume (EGV) of this novel TC-CCES system is 2.12 kW·h/m^3, lower than that in [27], which is 3.07 kW·h/m^3. The reason can be explained from Table 7. From the data on power distribution in energy recovery process in [27], the power output of the turbine train is derived from two sources: (1) the energy stored by the compression process, and (2) the energy supplied by extra fuel to heat the cold turbine output gas. The total power output of the turbine train is 254.82 kW, and the extra fuel input is 217.86 kW, which accounts for 85.5% of the whole power output, so the net electricity power supplied by the storage process is very low, only 36.96 kW, which accounts for 14.5% of the total power output. Meanwhile, the utilization rate of fuel exergy is as high as 89%. In the novel TC-CCES system with heat pump, no extra fuel energy is input during energy recovery process, but the heat pump requires electricity power equal to 44.24 kW, which accounts for 28.1% of total output. During the turbine train work in the energy recovery process, and the energy stored by the compression process is supplied to the turbine train making the energy storage efficiency higher than in [27]. The utilization of heat exergy in TR is 55.1% because of the large use of fuel, the exergy utilization is higher than thermal for the part of using turbine re-heater instead of fuel on the reheating the turbines process, but energy storage efficiency, exergy efficiency and round-trip efficiency of the TC-CCES system are larger than that in [27]. According to Eq. (7) and Eq. (16), the value of EGV mainly depends on two parts: (1) the net electricity power output and (2) the density difference between the inlet, and outlet CO_2 in the storage reservoir. In the prior TC-CCES, the value of the density difference is much smaller than that in the TC-CCES system. Hence, the value of EGV in [27] is larger than that in the TC-CCES system. In order to use the TC-CCES, a large underground storage reservoir volume is needed, consistent with use of an aquifers or solution-mined caverns.

The exergy destruction percentages for the various system components are depicted in Fig. 4. From Fig. 4, one sees for the TC-CCES system that 44.91% of the irreversibility occurs in TR, 20.46% in HP, 16.63% in IC, 4.95% in C, 4.41% in T, 4.13% in HR, 3.17% in PC, and 1.32% in LR.

5.2 Sensitivity analysis

From the thermodynamic performance analysis, we find the novel TC-CCES system has high exergy efficiency, energy storage efficiency and round-trip efficiency. The main properties controlling the efficiency and EGV of the system are, the energy storage pressure (inlet pressure of HR), energy recovery pressure (inlet pressure of the T1), and pressure of the LR (outlet pressure of the T3) [44]. We conducted a sensitivity analysis with parameter ranges listed in Table 8 to quantify how performance can be improved.

5.2.1 Effect of energy storage pressure

It is noted that the pressure drop across the high-pressure throttle valve maintains 2 MPa and stays almost constant. When the energy storage pressure varies from 15 MPa to 25 MPa, the energy recovery pressure will also change, varying from 13 MPa to 23 MPa with a 1 MPa increment, while the pressure of LR is set as 1 MPa, and other parameters remain unchanged. As shown in Fig. 5, the overall pressure of the storage system plays a large role in the TC-CCES efficiency. Specifically, the value of η_{RT}, η_{ES}, and η_{EX} increase as energy storage pressure increases. Note that there is a crossover of η_{RT} and η_{EX} at a pressure of 20 MPa. This occurs because an increase in the energy storage pressure leads to an increase of net energy output during the energy recovery process, which can increase the value of EGV. The required volume of the HR is reduced by high energy storage pressure, whereas variation of the power output is contrary to that of the required volume. Hence, EGV will rise along with increase of the energy storage pressure.

Fig. 6 depicts the changes in the power of the compressor train, turbine train, and heat pump with the changes in energy storage pressure. As the energy storage pressure increases, the output of the heat pump gently increases, whereas the net output of compressor and turbine have stronger growth trends that level off at high pressures. The reason why growth is gradually slowing down is that for the compressor train, as the storage pressure increases, the CO_2 working fluid changes from a trans-critical state to a supercritical state. Due to the physical properties of the supercritical CO_2 itself, the power consumed by the compressor will reduce and the power output by the turbine will reduce, so both growth rate of the power consumption of the compressor train and output power of the turbine train gradually decreases. Energy storage pressure also controls the exergy destruction percentage in the main components. In Fig. 7, it is seen that exergy destruction occurs mainly in TR, HP, and IC, with the largest exergy destruction coming from TR. The inlet pressure of the turbine will grow with the rise of the energy storage pressure, and all other setting parameters held constant. Hence, the temperature difference of the heat exchangers will grow, therefore, the exergy destruction percentage increases from 62.42 kW to 83.89 kW in IC, and decreases from 184.6 kW to 176.3 kW in TR. The exergy destruction rate occurring in C, T, and HR have a similar increasing trend with rise in energy storage pressure, which is caused by the pressure difference between the inlet and outlet of each component; the higher the pressure drop is, the larger the exergy destruction will become.

5.2.2 Effect of energy recovery pressure

It is noted that when the pressure of energy recovery changes from 8 MPa to 15 MPa with 1 MPa increment, the energy storage pressure and the pressure of LR are set to 17 MPa and 1 MPa while the other setting parameters listed in Table 3 remain unchanged . In Fig. 8 it is illustrated the dependence of η_{RT}, η_{ES}, and EGV with the energy recovery pressure. The value of η_{ES} increases from 41.63% to 58.41%, the value of η_{RT} rises from 52.54% to 62.16%, the value of η_{EX} has a gentle change from 66.9% to 68.87%. What's more, the growth in energy recovery pressure will result in a rise in the output power of the turbine train, the pressure drop will decline which causes a smaller volume required for HR. Therefore, the EGV will increase with higher energy recovery pressure.

The effects of energy recovery pressure on the power in the compressor train, turbine train and heat pump are shown in Fig. 9. The power of the compressor train is constant and the power of the turbine train increases rapidly from 124.82 to 157.06 kW with growth of the energy recovery pressure. In addition, the power of the heat pump mainly depends on the amount of heat exchange required for the reheating of the turbine during the energy recovery process, whereas it is independent of the energy recovery pressure. Therefore, the heat pump power requirement is almost constant in the energy recovery process.

Fig. 10 illustrates the influence of energy recovery pressure on the exergy destruction rate of the system components. The exergy destruction rate of TR and PC decline with larger energy recovery pressure in the TC-CCES system, which varies from 186.1 kW to 183.6 kW in TR and 21.17 kW to 12.96 kW in PC. The reason is that the exergy destruction of TR and PC are mainly controlled by their temperature differences. In fact, the temperature differences across TR and PC will be smaller with larger energy recovery pressure. Therefore, the exergy destruction in TR and PC will be smaller for greater energy storage pressure in the case that all other parameters remain unchanged. And it can be also found that the exergy destruction of other components change only slightly with energy recovery pressure.

5.2.3 Effects of pressure in LR

When the pressure in the low-pressure reservoir has a change from 1 MPa to 2 MPa, with a 0.2 MPa increment, the energy storage pressure and energy recovery pressure are set as 17 MPa and 15 MPa, respectively, and other setting parameters are kept constant. In Fig. 11 it can be observed that as with higher pressure of LR, the values of η_{RT}, η_{ES}, η_{EX}, and EGV of the TC-CCES system are reduced. The maximum change is in η_{ES} which decreases from 58.41% to 37.6%, the second largest change is in η_{RT} which reduces from 66.16% to 49.3%, the value of η_{EX} has a gentle decline of 3.54%. When CO_2 in the LR is in a trans-critical state, the pressure change of LR has a greater effect on the change of the CO_2 density, so the volume change of the gas storage reservoir becomes larger, the EGV decreases larger. Fig. 12 shows the influence of the pressure of LR on the power of the compressor train, turbine train, and heat pump. With increase of pressure of the LR, the power of the turbine train decreases sharply from 157.06 to 117.16 kW. The reason is that in the case of other design parameters unchanged, the increase of pressure of LR causes the power of each stage of the turbine to be reduced and the net output of the system to be reduced, while the consumption of the system compressor remains constant.

The effects of the various components on exergy destruction rate as a function of the pressure of LR are shown in Fig. 13. The analysis shows that the exergy destruction rates of TR and PC rise with growing pressure of LR, which increases from 184.5 to 192 kW in TR and from 1.3 to 14 kW in PC. The reason for this increase is that the outlet temperature of each turbine increases and the power of the turbine decreases with higher LR pressure and therefore the exergy destruction of TR and PC increases. In addition, the pressure difference becomes larger in LR, which varies from 5.4 to 46.1 kW, as pressure in LR increases, making the exergy destruction rate of LR increase.

6. Conclusions

This study contained a thermodynamic analysis of a novel, fossil-fuel-free, TC-CCES system that uses two saline aquifers or caverns for storing compressed CO_2 and that includes two thermal storage tanks and a heat pump system as thermal storage and recovery systems, respectively and an investigation of its operational behavior and efficiency. The main conclusions are:

(1) Under a typical trans-critical operation condition, the round-trip efficiency is 66%, energy storage efficiency is 58.41%, exergy efficiency is 67.89% and EGV is 2.12 $kW{\cdot}h/m^3$, which indicates a good thermodynamic performance of the novel TC-CCES system.

(2) Sensitivity analysis shows that higher energy storage pressure, energy recovery pressure and lower the pressure of LR will improve the four performance indicators including η_{RT}, η_{ES}, η_{EX} and EGV.

(3) By comparing the exergy destruction rate of the main components in the system, we find the exergy destruction rate of the heat exchangers accounts for a large proportion of exergy destruction with 49.3% in TR and 16.46% in IC, respectively. It indicates that significant potential improvement in system performance can be made by optimizing the turbine re-heater exchanger to reduce the exergy destruction rate.

We note finally that the operating efficiency of the system is good, the working parameters are not extreme during operation, and the requirements of the components in the system are reasonable suggesting it may be practical to build and operate this novel fossil-fuel-free trans-critical CO_2 energy storage system.

Acknowledgements

We thank the National Key Research and Development Program of China (Grant No.2017YFB0903601), the Double First-rate Construction Program of China, and Lawrence Berkeley National Laboratory supported by the U.S. Department of Energy under Contract No.DE-AC02-05CH11231.

References

[1] Qin, J.X., The Status and Prospect of New Energy and Renewable Energy in China. Material Science, Energy Technology and Power Engineering. 2018, Amer Inst Physics: Melville.

[2] P.S. Georgilakis, Technical challenges associated with the integration of wind power into power system, Renew. Sustain. Energy Rev. 12 (2008) 852-863.

[3] Wang, J., Qin, S., Jin, S., Estimation methods review and analysis of offshore extreme wind speeds and wind energy resources. Renewable & Sustainable Energy Reviews, 2015. 42: p. 26-42.

[4] Świerczyński, M., Teodorescu, R., Rasmunssen, C., Overview of the energy storage systems for wind power integration enhancement. IEEE International Symposium on Industrial Electronics. 2010.

[5] Chen, L., Dai, Y., Min, Y., Study on the Mechanism of Transient Voltage Stability of Wind Power With Power Electronic Interface. 2015 IEEE Pes Asia-Pacific Power and Energy Engineering Conference. 2015, New York.

[6] Castillo A, Gayme D F. Grid-scale energy storage applications in renewable energy integration: A survey[J]. Energy Conversion and Management, 2014, 87:885-894.

[7] B. Dursun, S. Alboyaci. The contribution of wind-hydro pumped storage systems in meeting Turkey's electric energy demand, Renew. Sustain. Energy Rev, 14 (2010) 1979-1988.

[8] I. Arsie, V. Marano, G. Nappi, G. Rizzo. A model of hybrid power plant with wind turbines and compressed air energy storage, in: Proceedings of the ASME Industrial Power Conf. Pts A and B, 2005, pp.987-1000.

[9] Aneke, M. and Wang, M. Energy storage technologies and real life applications–A state of the art review. Applied Energy, 2016,179, pp.350-377.

[10] Temple, J. The $2.5 trillion reason we can't rely on batteries to clean up the grid, MIT Technology Review, 2018, July 27, 2018. https://www.technologyreview.com/s/611683/ the-25- trillion-reason-we-cant-rely-on-batteries-to-clean-up-the-grid/

[11] Guo H, Xu Y, Chen H, Zhou X. Thermodynamic characteristics of a novel supercritical

compressed air energy storage system. Energy Convers Manage, 2016;115:167-77.

[12] Oldenburg CM, Pan L. Porous media compressed-air energy storage (PM-CAES): theory and simulation of the coupled wellbore-reservoir sysytem. Transpory Porous Med 2013;97(2): 201-221

[13] Jannelli E, Minutillo M, Lavadera AL, Falcucci G. A small-scale CAES (compressed air energy storage) system for stand-alone renewable energy power plant for a radio base station: a sizing-design methodology. Energy, 2014;78:313-22.

[14] C.Bullough, C.Gatzen, C.Jakiel, M.Koller, A.Nowi, S.Zunft, Advanced adiabatic compressed air energy storage for the integration of wnd, in: European Wind Energy Conf. London, UK, 2004.

[15] G. Grazzini, A.Milazzo, Thermodynamic analysis of CAES/TES system for renewable energy plants, Renew. Energy, 33 (2008)1998-2006.

[16] W.F. Pickard, N.j. Hansing, A.Q. Shen, Can large-scale advanced-adiabatic compressed air energy storage be justified economically in an age of sustainable energy, J. Renew. Sustain. Energy, 1 (2009)033102:1-033102:10.

[17] Cárdenas, B., Pimm, A.J., Kantharaj, B., Simpson, M.C., Garvey, J.A. and Garvey, S.D., 2017. Lowering the cost of large-scale energy storage: High temperature adiabatic compressed air energy storage. Propulsion and Power Research, 6(2), pp.126-133.

[18] Szablowski, L., Krawczyk, P., Badyda, K., Karellas, S., Kakaras, E. and Bujalski, W., 2017. Energy and exergy analysis of adiabatic compressed air energy storage system. Energy, 138, pp.12-18

[19] He, W., Luo, X., Evans, D., Busby, J., Garvey, S., Parkes, D. and Wang, J., 2017. Exergy storage of compressed air in cavern and cavern volume estimation of the large-scale compressed air energy storage system. Applied energy, 208, pp.745-757.

[20] Guo, H., Xu, Y., Chen, H. and Zhou, X., 2016. Thermodynamic characteristics of a novel supercritical compressed air energy storage system. Energy conversion and management, 115, pp.167-177.

[21] Liu JL, Wang JH. A comparative research of two adiabatic compressed air energy storage systems. Energy Convers Manage, 2016;108:566-78

[22] Yao E, Wang H, Wang L, Xi G, Marechal F. Thermo-economic optimization of a combined cooling, heating and power system based on small-scale compressed air energy storage. Energy Convers Manage, 2016; 118:377-86.

[23] Morgan, R., et al., Liquid air energy storage-Analysis and first results from a pilot scale demonstration plant. Applied Energy, 2015. 137(3): p. 845-853.

[24] HE Qing, WANG Lijian, ZHOU Qian, LU Chang, DU Dongmei, LIU Wenyi. Systematic optimization and thermodynamic analysis of liquefied air energy storage system. Energy, Vol.173, 2019.4.15: 162-173

[25] Wang M, Zhao P, Wu Y, Dai Y. Performance analysis of a novel energy storage system based on liquid carbon dioxide. Appl Therm Eng, 2015; 91:812-23.

[26] Wu Y, Hu D, Wang M, Dai Y. A Novel Transcritical CO_2 Energy Storage System.Journal of Xi’an Jiao Tong University, 2016.50 (3):45-49.

[27] Liu, H., He, Q., Borgia, A., Thermodynamic analysis of a compressed carbon dioxide energy storage system using two saline aquifers at different depths as storage reservoirs. Energy Conversion and Management, 2016. 127: p. 149-159.

[28] Buscheck, T.A., Bielicki, J.M., Edmunds, T.A., Hao, Y., Sun, Y., Randolph, J.B. and Saar, M.O. Multi-fluid geo-energy systems: Using geologic CO_2 storage for geothermal energy production and grid-scale energy storage in sedimentary basins. Geosphere, 2016. 12(3), pp.678-696.
[29] Ahmadi M H, Mehrpooya M, Pourfayaz F. Thermodynamic and exergy analysis and optimization of a transcritical CO_2 power cycle driven by geothermal energy with liquefied natural gas as its heat sink[J]. Applied Thermal Engineering, 2016, 109:640-652.
[30] Ahmadi M H , Mehrpooya M , Pourfayaz F . Exergoeconomic analysis and multi objective optimization of performance of a Carbon dioxide power cycle driven by geothermal energy with liquefied natural gas as its heat sink[J]. Energy Conversion and Management, 2016, 119:422-434.
[31] Ahmadi M H, Mohammadi A, Pourfayaz F, et al. Thermodynamic analysis and optimization of a waste heat recovery system for proton exchange membrane fuel cell using transcritical carbon dioxide cycle and cold energy of liquefied natural gas[J]. Journal of Natural Gas Science and Engineering, 2016, 34:428-438.
[32] Naseri A , Bidi M , Ahmadi M H , et al. Exergy Analysis of a hydrogen and water production process by a solar-driven transcritical CO_2, power cycle with Stirling engine[J]. Journal of Cleaner Production, 2017:S0959652617309228.
[33] Mercang Z M, Hemrle J, Kaufmann L, et al. Electrothermal energy storage with transcritical CO2 cycles[J]. Energy, 2012, 45(1):407-415.
[34] Zhang Y, Yang K, Hong H, et al. Thermodynamic analysis of a novel energy storage system with carbon dioxide as working fluid[J]. Renewable Energy, 2016, 99:682-697.
[35] Zhang XR, Wang GB. Thermodynamic analysis of a novel energy storage system based on compressed CO_2 fluid. Int J Energy Res, 2017; 41(10):1487-503.
[36] Arpagaus C, Bless F, Uhlmann M, et al. High temperature heat pumps: Market overview, state of the art, research status, refrigerants, and application potentials[J]. Energy, 2018, 152:S0360544218305759.
[37] Huang M, Liang X, Zhuang R. Experimental investigate on the performance of high temperature heat pump using scrool compressor. In:12th IEA Heat pump Cofference, Rotterdam;14-17 May,2017. P.1-8.
[38] NIST Standard Reference Database 23, NIST Thermodynamic and Transport Properties of Refrigerants and Refrigerant Mixtures PEFPROP, Version 9.0, 2010.
[39] Sarkar J. Cycle parameter optimization of vortex tube expansion transcritical CO_2 system[J]. International Journal of Thermal Science, 2009, 48(9): 1823-1828.
[40] Succar, Samir, Williams Robert H. Compressed air energy storage: theory, resources, and applications for wind power. Report no. 8. Princeton environmental institute; 2008.
[41] Kim YM, Lee JH, Kim SJ, Favrat D. Potential and evolution of compressed air energy storage: energy and exergy analyses. Entropy, 2012;14(8):1501-21.
[42] Liu H, He Q, Saeed SB. Thermodynamic analysis of a compressed air energy storage system through advanced exergetic analysis. J Renew Sustain Energy, 2016;8(3):034101.
[43] Wang L, Yang Y, Morosuk T, Tsatsaronis G. Advanced thermodynamic analysis and evaluation of a supercritical power plant. Energies, 2012;5(6):1850-63.
[44] Qing H, Yinping H, Hui L, et al. Analysis of exergy efficiency of a super-critical compressed carbon dioxide energy-storage system based on the orthogonal method[J]. PLOSONE, 2018, 13(4):e0195614.

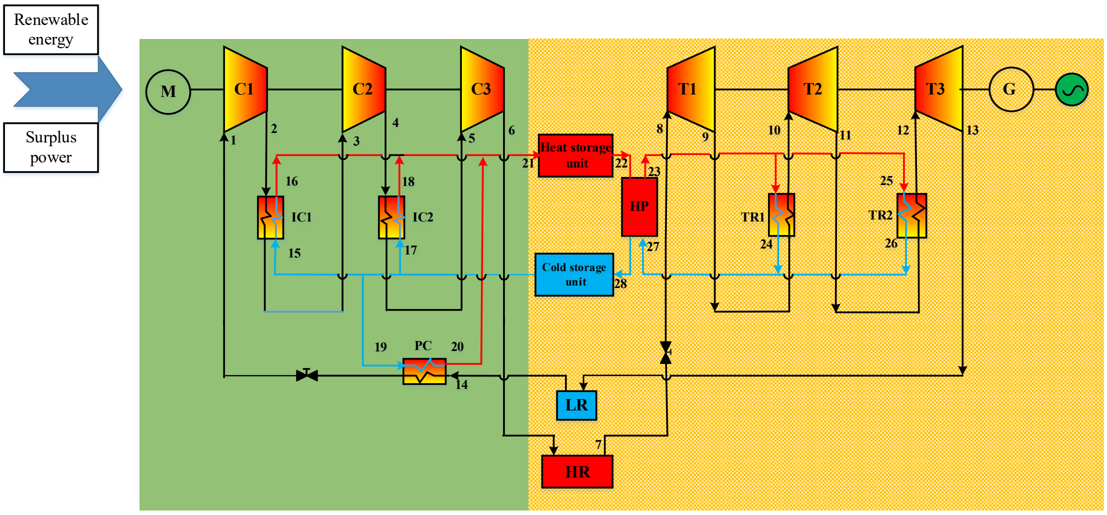

Fig. 1 Schematic of the TC-CCES system

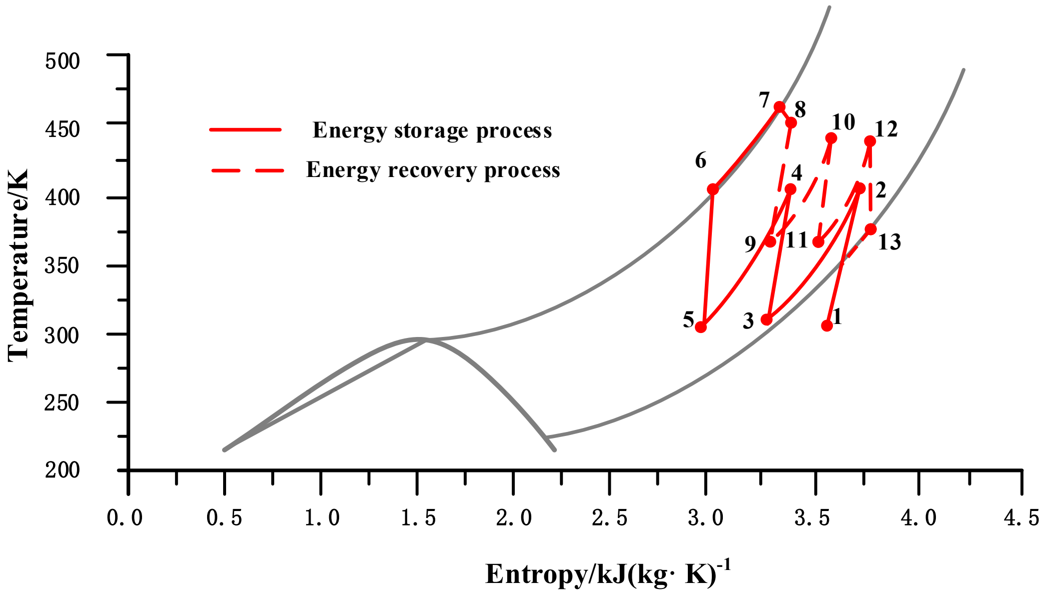

Fig. 2 T-S graph of the TC-CCES system

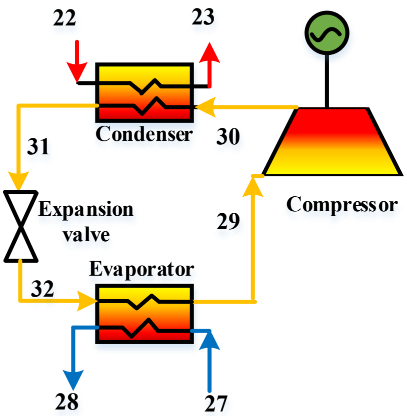

Fig. 3 Schematic of heat pump sub-system

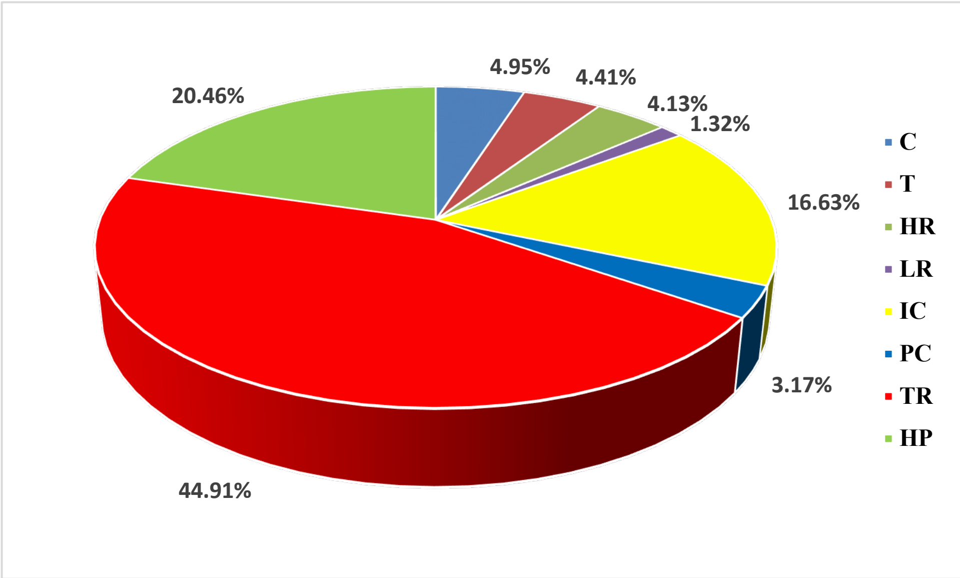

Fig. 4. The exergy destruction in the main components of the TC-CCES system.
C = compressor; T = turbine; HR = high-pressure reservoir; LR = low-pressure reservoir; IC = inter cooler of compressor; PC = pre-cooler; TR = turbine re-heater; HP = heat pump.

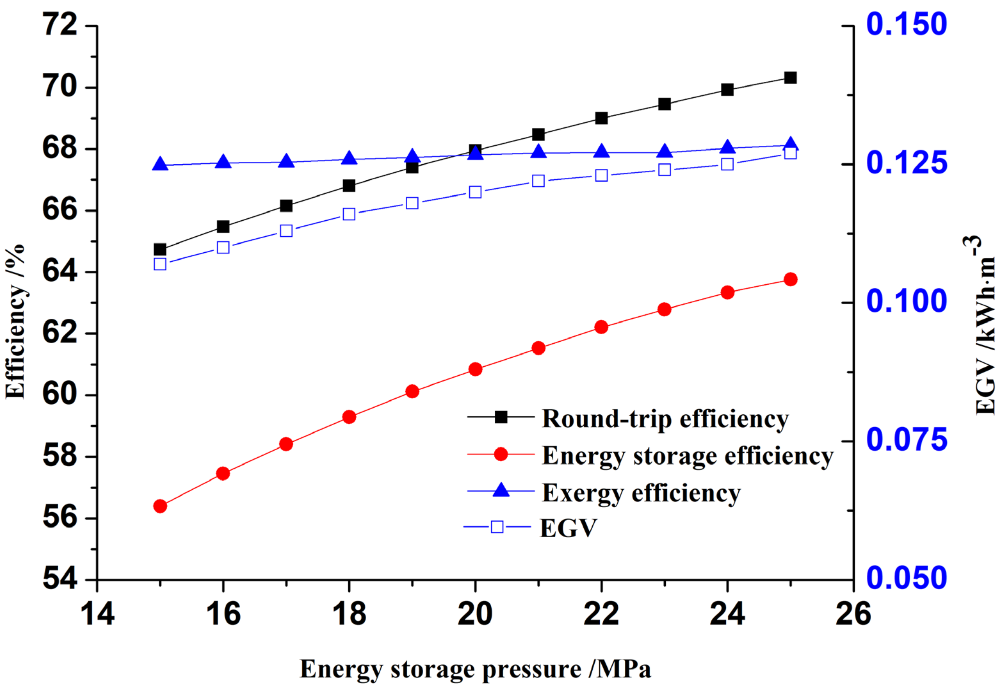

Fig. 5 Energy storage pressure control on system efficiency and EGV.

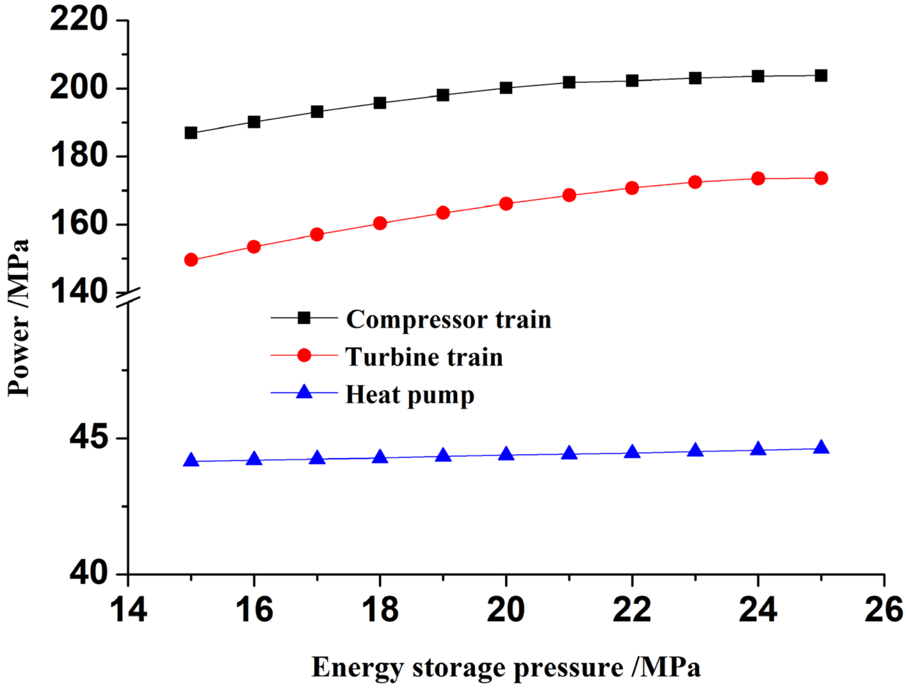

Fig. 6. Energy storage pressure control on power of compressor train, turbine train and heat pump

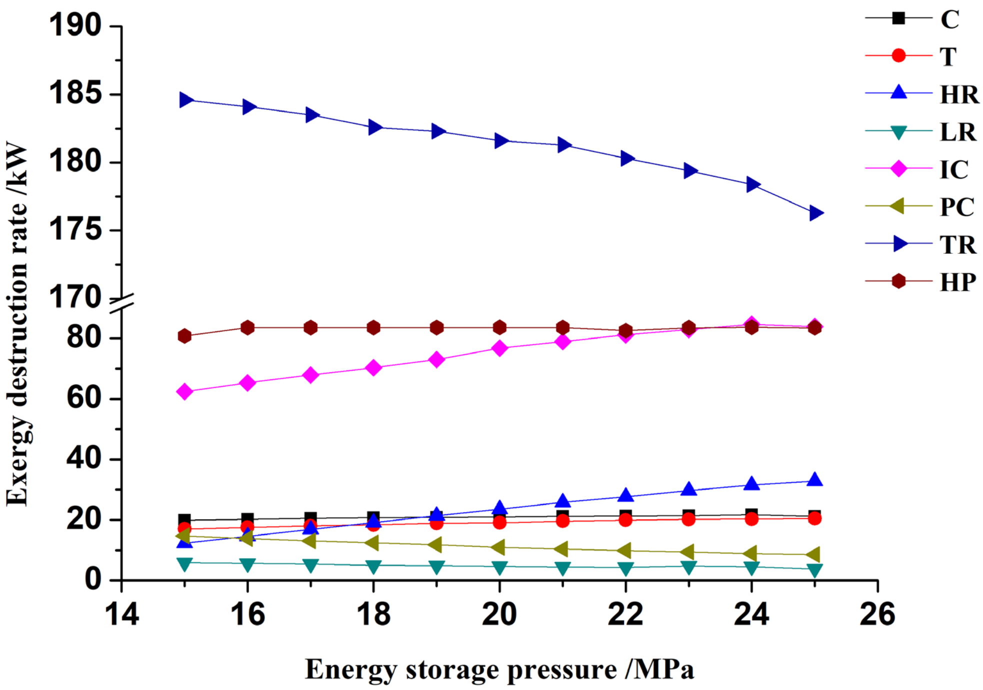

Fig. 7. Energy storage pressure control on exergy destruction rate.

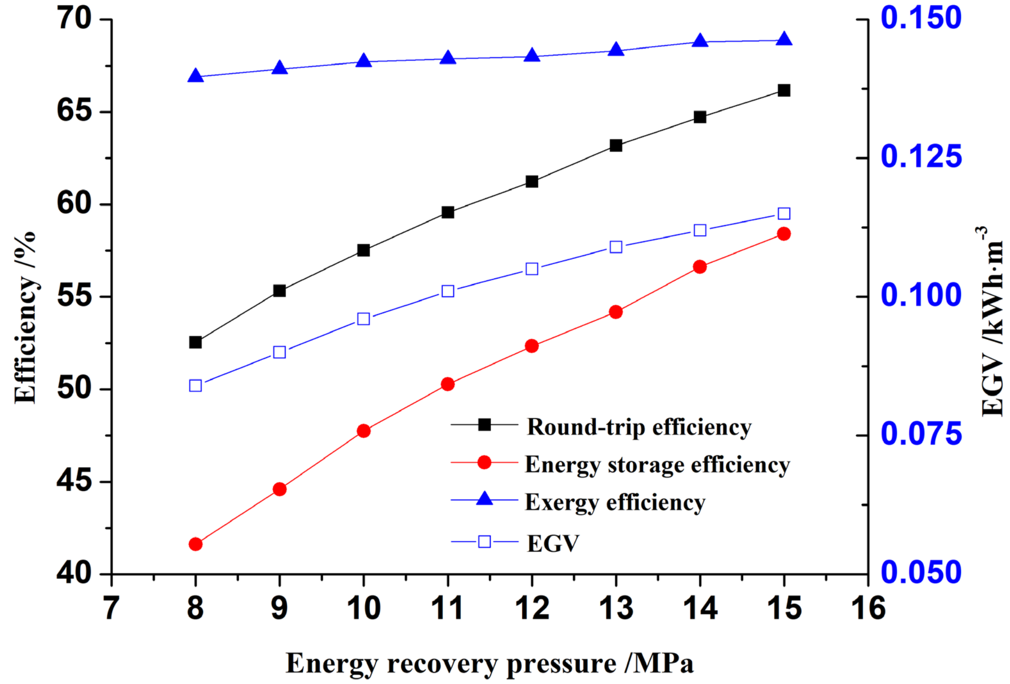

Fig. 8. Energy recovery pressure control on system efficiency and EGV.

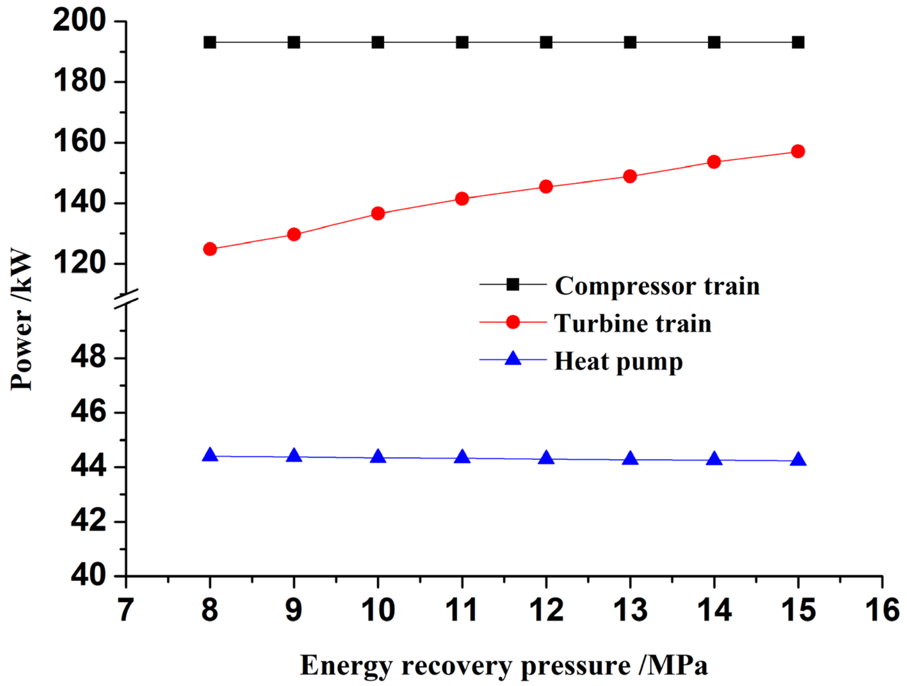

Fig. 9. Energy recovery pressure control on power of compressor train, turbine train and heat pump.

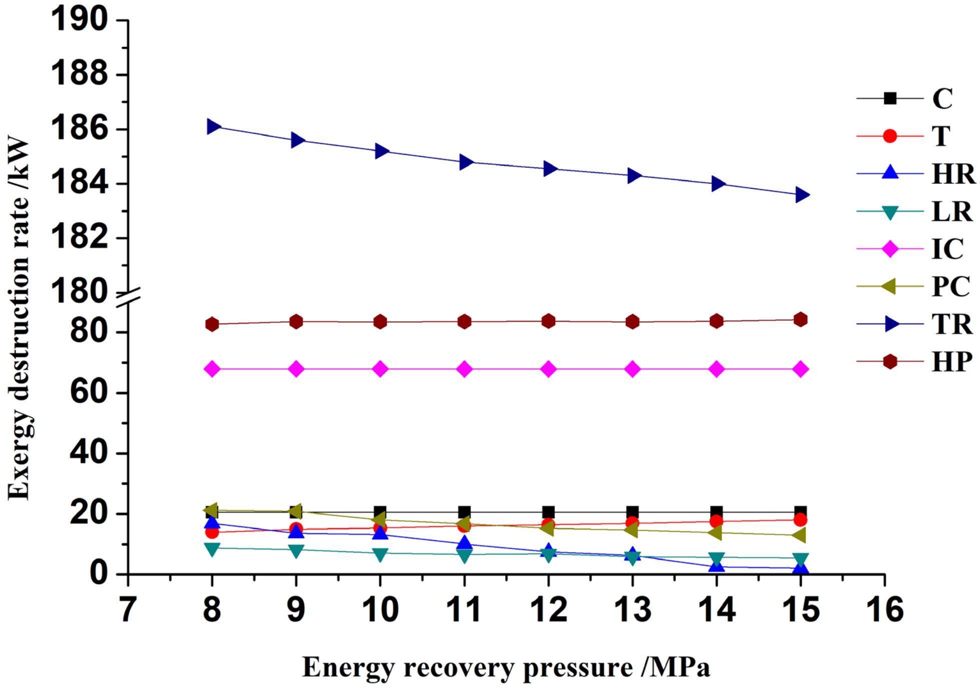

Fig. 10. Energy recovery pressure control on exergy destruction rate.

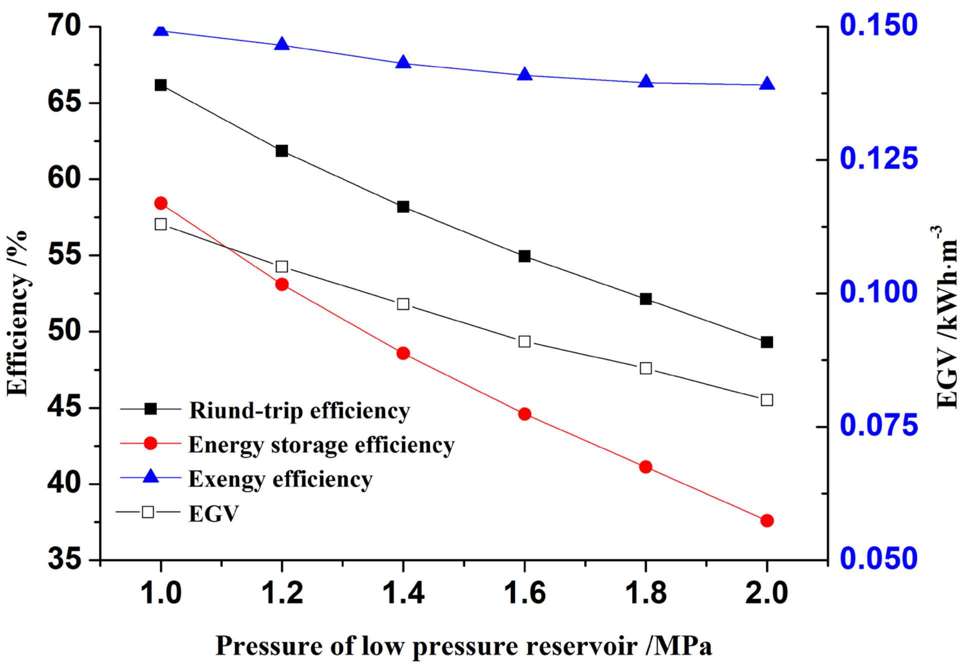

Fig. 11 Pressure of LR control on efficiency and EGV.

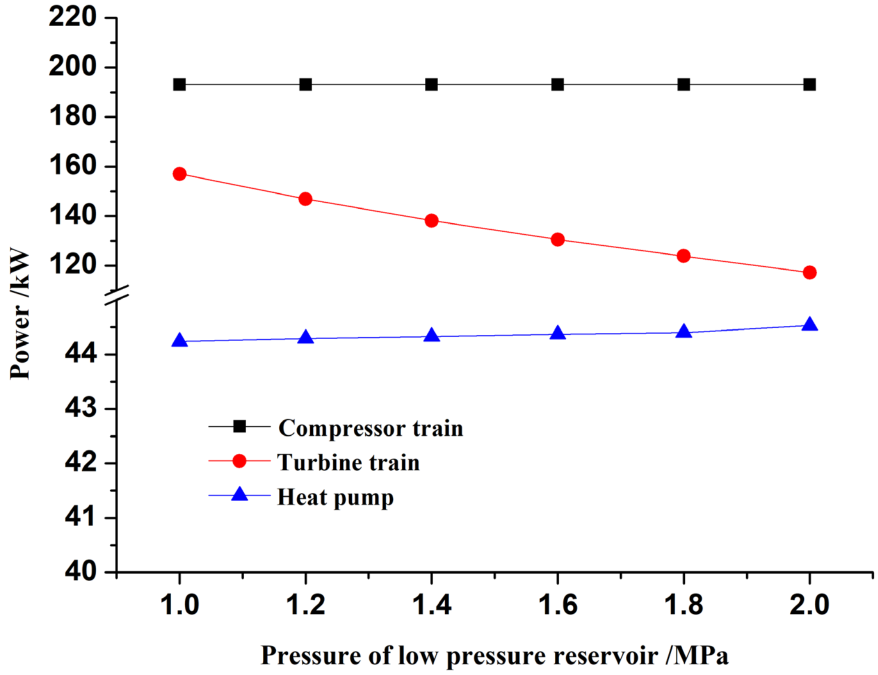

Fig. 12. Pressure of LR control on power of compressor train, turbine train and heat pump.

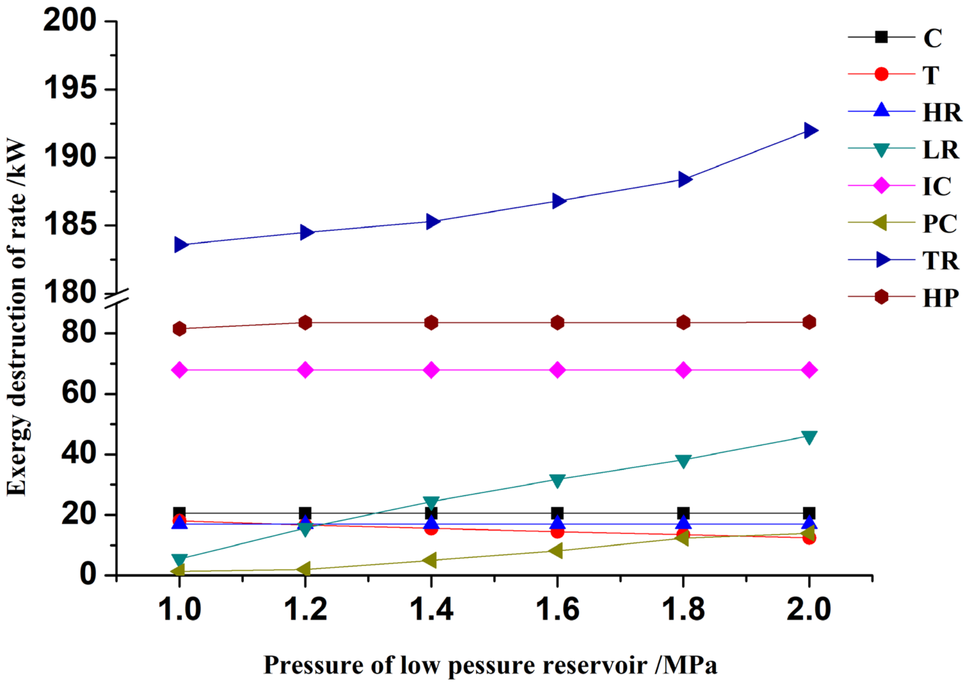

Fig. 13 Pressure of LR control on exergy destruction rate.

Table 1. Physical properties of R245fa.

Item	Value	Unit
Molecular formula	CHF2CH2CF3	
Critical temperature	427.15	K
Critical pressure	3.65	MPa
Boiling temperature	288.05	K

Table 2. Exergy calculation of components in the TC-CCES system

Component	$\dot{E}_{F,n}$	$\dot{E}_{P,n}$	$\dot{E}_{d,n}$
Compressor	W_c	$\dot{E}''_c - \dot{E}'_c$	$\dot{E}_{F,c} - \dot{E}_{P,c}$
Turbine	$\dot{E}'_T - \dot{E}''_T$	W_T	$\dot{E}_{F,T} - \dot{E}_{P,T}$
Heat exchanger	$\dot{E}'_{hot,HE} - \dot{E}''_{hot,HE}$	$\dot{E}''_{cold,HE} - \dot{E}'_{cold,HE}$	$\dot{E}_{F,HE} - \dot{E}_{P,HE}$
Storage reservoir	$\dot{E}'_{SC}$	$\dot{E}''_{SC}$	$\dot{E}_{F,SC} - \dot{E}_{P,SC}$
Valve	$\dot{E}'_V$	$\dot{E}''_V$	$\dot{E}_{F,V} - \dot{E}_{P,V}$

Table 3. Properties of the TC-CCES system

Item	Value	Unit
Ambient temperature	298.15	K
Inlet temperature of compressor	308.15	K
Depth of LR	100	m
Depth of HR	1700	m
Throttle valve pressure drop in energy recovery process	0.2	MPa
Throttle valve pressure drop in energy storage process	2	MPa
Inlet temperature of cooling water	298.15	K
Inlet pressure of cooling water	0.2	MPa
Inlet pressure of compressor	0.8	MPa
Outlet pressure of the third stage compressor	17	MPa
Outlet pressure of the third stage turbine	1	MPa
Isentropic efficiency of compressor	86	%
Isentropic efficiency of turbine	88	%

Table 4. Material stream parameters of TC-CCES system

Stream No.	Temperature (K)	Pressure(MPa)	Mass flow rate (kg/h)
1	308.15	0.8	3600
2	395.85	2.216	3600
3	308.15	2.216	3600
4	399.95	6.138	3600
5	308.15	6.138	3600
6	396.85	17	3600
7	447.65	17	3600
8	441.75	15	3600
9	363.39	6.084	3600
10	423.15	6.084	3600
11	352.44	2.467	3600
12	423.15	2.467	3600
13	357.29	1	3600
14	361.29	1	3600
15	298.15	0.2	829.4
16	385.85	0.2	829.4
17	298.15	0.2	1110
18	389.95	0.2	1110
19	298.15	0.2	781.2
20	351.30	0.2	781.2
21	377.75	0.2	2721
22	377.75	0.1	3600
23	433.15	0.2	5164
24	406.35	0.1	5164
25	433.15	0.2	5540
26	407.45	0.1	5540
27	406.95	0.1	10700
28	363.15	0.1	3600
29	406.65	0.68	3600
30	435.85	1.7	3600
31	387.75	1.1	3600
32	377.05	0.3	3600

Table 5. Results of the main components in the TC-CCES

Term	Unit	Value
C1 power	kW	73.77
C2 power	kW	68.14
C3 power	kW	51.23
T1 power	kW	49.18
T2 power	kW	52.21
T3 power	kW	55.67
Heat pump power	kW	44.24

Table 6. Results of the performance criteria of the TC-CCES

Item	Unit	TC-CCES	Ref.[27]
Energy storage efficiency	%	58.41	20.04
Round-trip efficiency	%	66.00	63.35
Exergy efficiency	%	67.89	53.02
EGV	kW·h/m^3	2.12	3.07

Table 7. The power distribution in recovery process of the TC-CCES

Item	Unit	TC-CCES	Ref.[27]
Whole electricity output	kW	157.48	254.82
Extra fuel input	kW	0	217.86
Consume electricity	kW	44.24	0
Net electricity recovered from storage	kW	113.24	36.96

Table 8. Ranges of parameters for the sensitivity analysis

Parameters	Unit	Range
Energy storage pressure	MPa	16-25
Energy recovery pressure	MPa	8-15
Pressure of LR	MPa	1.0-2.0

Nomenclature

T	Temperature (K)
P	Pressure (MPa)
W	Power (kW)
E	Electricity power (kW·h)
$\dot{Q}$	Heat transfer rate (kW)
C_p	Specific heat capacity at constant pressure (kJ/(kg K))
G	Geothermal gradient (K/km)
$\dot{m}$	Mass flow rate (kg/h)
V	Volume (m^3)
Z	Reservoir depth (m)
t	Time (h)
Greek symbols	
Δ	Change quantity

η	Efficiency
ρ	Density (kg/m^3)
Subscripts	
T	Turbine
C	Compressor
i	Stage of compressor
j	Stage of turbine
$'$	Inlet stream
$''$	Outlet stream
Abbreviations	
CO_2	Carbon dioxide
TC-CCES	Trans-critical compressed CO_2 energy storage
CCES	Compressed CO_2 energy storage
CAES	Compressed air energy storage
A-CAES	Adiabatic CAES
AA-CAES	Advanced adiabatic CAES
HP	Heat pump
HR	High-pressure reservoir
IC	Inner cooler exchanger
PC	Pre-cooler exchanger
TR	Turbine re-heater exchanger
C	Compressor
T	Turbine
LR	Low-pressure reservoir